Prediction of Airfoil Characteristics With Higher Order Turbulence Models

Thomas B. Gatski
Aerodynamic and Acoustic Methods Branch
NASA Langley Research Center, Hampton, VA 23681-0001, USA

ABSTRACT

The assessment of turbulence model performance in predicting flow fields that are directly relevant to industrial needs has become increasingly important. In aerodynamics, many problems exist for which the performance of some turbulence models is ambiguous at best and incorrect at worst. The application of many different turbulence models to a particular problem is a lengthy process that can lead to confusing results simply as a result of the volume of data produced. Given the motivation to develop turbulence models that do have some applicability to solving industry's problems, this study focuses on the prediction of airfoil characteristics, including lift and drag, over a range of Reynolds numbers. Two different turbulence models, which represent two different types of models, are tested. The first is a standard isotropic eddy-viscosity two-equation $K-\varepsilon$ model, and the second is an explicit algebraic stress model (EASM). The EASM model is an extension of the $K-\varepsilon$ model because it introduces nonlinear dependency of the Reynolds stresses on the mean strain and rotation-rate tensors and, therefore, better accounts for the turbulent stress anisotropy more effectively. The turbulent flow field over a general-aviation airfoil (GA(W)-2) at three Reynolds numbers ranging from 2.1×10^6 to 6.3×10^6 is studied. Experimental pressure coefficients are compared with model predictions for $Re = 4.3 \times 10^6$. At each Reynolds number, predicted lift and drag values at different angles of attack are compared with experimental results, and predicted variations of stall locations with Reynolds number are compared with experimental data. Finally, the size of the separation zone predicted by each model is analyzed, and correlated with the behavior of the lift coefficient near stall. In summary, the EASM model is able to predict the lift and drag coefficients over a wider range of angles of attack than the $K-\varepsilon$ model for the three Reynolds numbers studied. However, both models are unable to predict the correct lift and drag behavior near the stall angle, and for the $Re = 2.1 \times 10^6$ case, the $K-\varepsilon$ model did not predict separation on the airfoil near stall.

I INTRODUCTION

The optimization of the performance and, therefore, the design of wing configurations is a challenging task that requires efficient use of numerical prediction techniques. In fact, an accurate predictive technique is a mandatory requisite. The purpose of this study is to assess the predictive capabilities of two types of turbulence models for the simpler two-dimensional airfoil configurations. The two types of models represented are an isotropic eddy-viscosity $K-\varepsilon$ model and an explicit algebraic stress model (EASM). They are applied to the flow over a general-aviation airfoil at various angles of attack and Reynolds numbers.

One problem with this type of study is the lack of detailed information in regard to the experimental setup, as well as the lack of necessary information about initial and inflow conditions. Nevertheless, some reports exist that provide sufficient information so that a study such as the one outlined here can be performed. One such study[1] details the aerodynamic characteristics of a 13-percent-thick general-aviation airfoil at various angles of attack and Reynolds numbers; the results of this study are used here to determine the ability of the models to predict some characterizing features of airfoil flows, such as the lift and drag coefficients and the pressure coefficient distributions at various flow conditions.

Other studies have examined the performance of $K-\varepsilon$ and algebraic stress models in predicting the aerodynamic characteristics of airfoil flows. Although the exact form of the two-equation models and ASM's differs between these studies (as well as this one), the intent is to examine whether the increased physics introduced into the ASM have a significant impact on the results. Because the ASM represents stress anisotropy effects better, its utilization should give some indication of whether a full Reynolds stress closure is worthwhile. Davidson and Rizzi[2] applied a two-equation model and an ASM to the ONERA-A airfoil flowfield at a single chord Reynolds number Re of 2.1×10^6. Their results showed that the ASM predicted the variation of C_l and the stall location better than the $K-\varepsilon$ model (and the Baldwin-Lomax model, which was also tested). In addition, the calculated pressure and skin-friction coefficients agreed very well with the experimental results.

Recently, Davidson[3] performed a follow-on study with a $K-\varepsilon$ and a Reynolds stress model at the same conditions as the Davidson and Rizzi work. Once again, the higher order model outperformed the isotropic eddy-viscosity $K-\varepsilon$ model. No stall was predicted by the $K-\varepsilon$ model, whereas stall location was accurately predicted by the Reynolds stress model, as were the velocity profiles on the airfoil and in the wake.

Lien and Leschziner[4] compared the performance of a $K-\varepsilon$, a Reynolds stress, and a nonlinear $K-\varepsilon$ (ASM) model on the ONERA-A airfoil as well, at the same chord Reynolds number used in the Davidson studies. Their study included the development of an improved ASM and Reynolds stress model to better predict the flow field. Their results suggested that the Reynolds stress model outperforms both the $K-\varepsilon$ and nonlinear $K-\varepsilon$ models in predicting the aerodynamic characteristics of the airfoil.

In the present study, the comparisons include the effects of Reynolds-number variation. In this study, no attempt is made to optimize the models for better predictive capabilities; the $K-\varepsilon$ model of Speziale *et al.*[5] and an ASM of Gatski and Speziale[6] are used. The algebraic stress model[6] is an explicit polynomial representation that is discussed in the next section. Comparisons of predicted and measured pressure coefficients are shown at two angles of attack at $Re = 4.3 \times 10^6$. For $Re = 2.1 \times 10^6$, 4.3×10^6, and 6.3×10^6, the variation of lift and drag coefficients C_l and C_d is shown as a function of angle of attack α and C_l, respectively. The variation of stall angle with Reynolds number is also examined, and the predicted results are compared with experimental results. Finally, to better understand the physics behind the stall-angle variation predicted by the $K-\varepsilon$ model and the EASM, comparative plots of separation-zone size are shown for the three Reynolds numbers. These results provide an indication of the capabilities of the models, and a direction for the next step in evaluating model performance and, ultimately, in improving the models.

II Theoretical Formulation

The mean quantities of an incompressible turbulent flow are obtained from a solution of the Reynolds-averaged Navier-Stokes equations given in nondimensional form as

$$\frac{\partial \overline{u}_j}{\partial x_j} = 0 \tag{1}$$

$$\frac{\partial \overline{u}_i}{\partial t} + \overline{u}_j \frac{\partial \overline{u}_i}{\partial x_j} = -\frac{\partial \overline{p}}{\partial x_i} + \frac{1}{Re}\frac{\partial \overline{\sigma}_{ij}}{\partial x_j} - \frac{\partial \overline{u_i' u_j'}}{\partial x_j} \tag{2}$$

where $\overline{u}_i$ and $\overline{p}$ are the mean velocity and pressure, respectively, and Re is the Reynolds number based on free-stream conditions and airfoil chord. The right-hand side of the equation also contains both the viscous stress tensor $\overline{\sigma}_{ij}$, which is proportional to the mean strain rate, and the turbulent second-moment correlation tensor $\tau_{ij} \equiv \overline{u_i' u_j'}$, which requires closure.

In the incompressible formulation for the mean motion, only the turbulent second-moment Reynolds stress tensor needs to be modeled. For the higher order closures,

it is best to begin with the transport equation for the τ_{ij} correlation:

$$\frac{\partial \tau_{ij}}{\partial t} + \frac{\partial}{\partial x_k}\left(\overline{u}_k \tau_{ij}\right) = \bar{P}_{ij} + \Pi^d_{ij} - \varepsilon_{ij} + \frac{\partial \bar{D}^t_{ijk}}{\partial x_k} + \nu \frac{\partial^2 \tau_{ij}}{\partial x_k \partial x_k} \tag{3}$$

where the right-hand side represents the rate of change of τ_{ij} produced by the turbulent production $\bar{P}_{ij}$, the deviatoric part of the pressure strain-rate correlation Π^d_{ij}, the turbulent dissipation rate ε_{ij}, and the turbulent diffusion $\bar{D}^t_{ijk}$. These terms are given by

$$\bar{P}_{ij} = -\tau_{ik}\frac{\partial \overline{u}_j}{\partial x_k} - \tau_{jk}\frac{\partial \overline{u}_i}{\partial x_k} \tag{3a}$$

$$\Pi^d_{ij} = \overline{p'\left(\frac{\partial u'_i}{\partial x_j} + \frac{\partial u'_j}{\partial x_i}\right)} \tag{3b}$$

$$\varepsilon_{ij} = \frac{2}{3}\varepsilon\delta_{ij} = 2\nu\overline{\frac{\partial u'_i}{\partial x_k}\frac{\partial u'_j}{\partial x_k}} \tag{3c}$$

and

$$\bar{D}^t_{ijk} = -[\overline{u''_i u''_j u''_k} + \overline{p'(u'_i\delta_{jk} + u'_j\delta_{ik})}] \tag{3d}$$

In the incompressible formulation, the deviatoric part of the dissipation rate is generally absorbed into the pressure-strain correlation to account for any anisotropic dissipation effects. However, models for the anisotropic dissipation rate ε_{ij} can be derived that negate this assimilation into the pressure-strain correlation.[7, 8] When the deviatoric part of the tensor dissipation rate is assimilated into the pressure-strain correlation, the isotropic dissipation rate ε is obtained from a modeled transport equation.

The common high-Reynolds-number form of the isotropic solenoidal dissipation-rate equation that is used is given by

$$\frac{\partial \varepsilon}{\partial t} + \frac{\partial}{\partial x_j}\left(\overline{u}_j \varepsilon\right) = \bar{\mathcal{P}}_\varepsilon - \bar{\mathcal{D}}_\varepsilon + \frac{\partial}{\partial x_j}\bar{\mathcal{D}}^t_{\varepsilon j} + \nu\frac{\partial^2 \varepsilon}{\partial x_j \partial x_j} \tag{4}$$

with

$$\bar{\mathcal{P}}_\varepsilon = -C_{\varepsilon 1}\frac{\varepsilon}{K}\tau_{ij}\frac{\partial \overline{u}_i}{\partial x_j} \tag{4a}$$

and

$$\bar{\mathcal{D}}_\varepsilon = C_{\varepsilon 2}\frac{\varepsilon^2}{K} \tag{4b}$$

where the first and second terms on the right side are the production and destruction of dissipation, respectively, and the last term is the viscous diffusion. The turbulent dissipation-rate diffusion term is modeled for the two-equation formulation used in this study as

$$\bar{\mathcal{D}}^t_{\varepsilon j} = \frac{\nu_t}{\sigma_\varepsilon}\frac{\partial \varepsilon}{\partial x_j} \tag{5}$$

The closure constants $C_{\varepsilon 1}$, $C_{\varepsilon 2}$, and σ_ε must be specified to complete the closure.

This brief outline completes the specification of the transport equations for the solution of the second-moment closure model. To this point, no specific models have been proposed for terms such as the pressure-strain correlation or turbulent diffusion. Many models exist in the literature; the reader is referred to the many review articles on the subject.[9–12]

From an engineering standpoint, this second-moment formulation is not without risk. Extensive computer resources and sophistication are necessary in implementing and numerically solving these equations over a two-equation formulation; furthermore no unambiguous assessment has been made of the range of validity of the models, which is, of course, unfortunate because these equations represent the inclusion of extensive physics and mathematical rigor that should lead to improved predictive technology. For this reason, an intermediary level can be introduced into the hierarchy of closure models that incorporates the key features of the second-moment closures but does not involve more effort than a simple isotropic eddy-viscosity two-equation model.

An effective compromise between the full second-moment closure and the two-equation model is the ASM . This approach extracts an algebraic relationship between the turbulent Reynolds stress and mean velocity field from the Reynolds stress formulation just discussed. The models are derivable from equilibrium hypotheses imposed on both the convective and diffusive terms. The convective equilibrium hypothesis is represented through the stress anisotropy tensor

$$b_{ij} = \frac{\left(\tau_{ij} - \frac{2}{3}K\delta_{ij}\right)}{2K} \tag{6}$$

and is given by

$$\frac{Db_{ij}}{Dt} \equiv \frac{D\tau_{ij}}{Dt} - \frac{\tau_{ij}}{K}\frac{DK}{Dt} = 0 \tag{7}$$

where $K = \tau_{ii}/2$. The equilibrium hypothesis for the diffusive terms is given by

$$\frac{\partial}{\partial x_k}\left(\bar{D}^t_{ijk} + \nu\frac{\partial^2\tau_{ij}}{\partial x_k \partial x_k}\right) = 0 \tag{8}$$

If we use these constraints, as well as the definition of the stress anisotropy, and consider the fact that the mean velocity gradient is the sum of the strain- and rotation-rate tensors ($\overline{S}_{ij}$ and $\overline{W}_{ij}$, respectively), then Equation (7) can be expanded as

$$\begin{aligned}(\bar{\mathcal{P}} - \varepsilon)b_{ij} = -\frac{2}{3}K\overline{S}_{ij} - K\left(b_{ik}\overline{S}_{jk} + b_{jk}\overline{S}_{ik} - \frac{2}{3}b_{mn}\overline{S}_{mn}\delta_{ij}\right) \\ - K(b_{ik}\overline{W}_{jk} + b_{jk}\overline{W}_{ik}) + \tfrac{1}{2}\Pi^d_{ij}\end{aligned} \tag{9}$$

where $\bar{\mathcal{P}} = \bar{P}_{ii}/2$, $\overline{S}_{ij} = (\partial\overline{u}_i/\partial x_j + \partial\overline{u}_j/\partial x_i)/2$, and $\overline{W}_{ij} = (\partial\overline{u}_i/\partial x_j - \partial\overline{u}_j/\partial x_i)/2$. This relation is the traditional starting point for the algebraic stress formulation. The pressure-strain correlation model Π^d_{ij} of Speziale, Sarkar, and Gatski (SSG)[13] is used in Equation (9) to close the equation.

For a two-dimensional flow, the exact integrity basis polynomial representation[6] of Equation (9) is given by

$$\begin{aligned}\tau_{ij} = \frac{2}{3}K\delta_{ij} - 2\nu_t^* \Big[\overline{S}_{ij} + \frac{\alpha_2 K}{\varepsilon}\Big(\overline{S}_{ik}\overline{W}_{kj} + \overline{S}_{jk}\overline{W}_{ki}\Big) \\ - 2\frac{\alpha_3 K}{\varepsilon}\Big(\overline{S}_{ik}\overline{S}_{kj} - \frac{1}{3}\overline{S}_{kl}\overline{S}_{kl}\delta_{ij}\Big)\Big]\end{aligned} \tag{10}$$

where

$$\nu_t^* = C_\mu^* \frac{K^2}{\varepsilon} \tag{11}$$

$$C_\mu^* = \frac{3(1+\eta^2)}{3+\eta^2+6\zeta^2\eta^2+6\zeta^2}\alpha_1 \tag{12}$$

$$\eta = \frac{\alpha_3 K}{\varepsilon}(\overline{S}_{ij}\overline{S}_{ij})^{1/2}, \quad \zeta = \frac{\alpha_2 K}{\varepsilon}(\overline{W}_{ij}\overline{W}_{ij})^{1/2} \tag{12a}$$

$$\alpha_1 = \left(\frac{4}{3} - C_2\right)\frac{g}{2}, \quad \alpha_2 = (2 - C_4)\frac{g}{2}, \quad \alpha_3 = (2 - C_3)\frac{g}{2}, \quad g = \frac{1}{\frac{C_1}{2} + C_5 - 1} \tag{12b}$$

For the SSG model,[13] these coefficients are

$$C_1 = 6.8, \quad C_2 = 0.36, \quad C_3 = 1.25, \quad C_4 = 0.40, \quad C_5 = 1.88 \tag{13}$$

The application of the model to a variety of compressible bump and airfoil flows[14] has shown that its robustness is diminished by using the C_μ^* coefficient given in Equation (12). The robustness diminishes because during the initial transient phases and in the free-stream region the value of C_μ^* attains values $< 0.2\alpha_1 \approx 0.023$. This low value of C_μ^* causes regions of high shear to form to maintain the turbulence, which in turn leads to numerical instabilities. To avoid these problems, a modified form of Equation (10) is used:

$$\begin{aligned}\tau_{ij} = \tfrac{2}{3}K\delta_{ij} - 2\nu_t^*\overline{S}_{ij} \\ - 2\nu_t^{**}\frac{K}{\varepsilon}\Big[\alpha_2\Big(\overline{S}_{ik}\overline{W}_{kj} + \overline{S}_{jk}\overline{W}_{ki}\Big) - 2\alpha_3\Big(\overline{S}_{ik}\overline{S}_{kj} - \frac{1}{3}\overline{S}_{kl}\overline{S}_{kl}\delta_{ij}\Big)\Big]\end{aligned} \tag{14}$$

where C_μ^* is now given by[15]

$$C_\mu^* = \frac{3(1+\eta^2) + 0.2(\eta^6+\zeta^6)}{3+\eta^2+6\zeta^2\eta^2+6\zeta^2+\eta^6+\zeta^6}\alpha_1 \tag{15}$$

and ν_t^{**} is now introduced and defined by

$$\nu_t^{**} = C_\mu^{**} \frac{K^2}{\varepsilon} \tag{16}$$

with

$$C_\mu^{**} = \frac{3(1+\eta^2)}{3+\eta^2+6\zeta^2\eta^2+6\zeta^2+\eta^6+\zeta^6}\alpha_1 \tag{17}$$

For large values of η and ζ, C_μ^* and C_μ^{**} are limited by $0.2\alpha_1$ and 0, respectively. In near equilibrium conditions, Equation (15) and (17) reduce to the value given in Equation (12).

The nonlinear algebraic constitutive equation given in Equation (14) is then coupled with an incompressible two-equation formulation. For the $K-\varepsilon$ formulation, the governing equations are subsets of the second-order formulation shown earlier in Equation (3) and (4). These governing equations are given by[15]

$$\frac{DK}{Dt} = \bar{\mathcal{P}} - \varepsilon + \frac{\partial}{\partial x_k}\left[\left(\nu + \frac{\nu_{tl}}{\sigma_k}\right)\frac{\partial K}{\partial x_k}\right] \tag{18}$$

and

$$\frac{D\varepsilon}{Dt} = C_{\varepsilon 1}\frac{\varepsilon}{K}\bar{\mathcal{P}} - C_{\varepsilon 2} f \frac{\varepsilon^2}{K} + \frac{\partial}{\partial x_k}\left[\left(\nu + \frac{\nu_{tl}}{\sigma_\varepsilon}\right)\frac{\partial \varepsilon}{\partial x_k}\right] \tag{19}$$

with

$$\nu_{tl} = C_{\mu l}\frac{K^2}{\varepsilon} \tag{19a}$$

$$f = \left[1 - \exp\left(-\frac{y^+}{5.5}\right)\right]^2, \quad y^+ = \frac{y u_\tau}{\nu} \tag{19b}$$

and

$$C_{\mu l} = 0.081, \quad \sigma_k = 1.0, \quad C_{\varepsilon 1} = 1.44, \quad C_{\varepsilon 2} = 1.83$$

$$\sigma_\varepsilon = \frac{\kappa^2}{(C_{\varepsilon 2} - C_{\varepsilon 1})\sqrt{C_{\mu l}}}, \quad \kappa = 0.41 \tag{19c}$$

where u_τ is the shear velocity and y is taken as the distance normal to the surface.

III RESULTS AND DISCUSSION

An isotropic eddy-viscosity two-equation model and a nonlinear algebraic stress model are evaluated based on their performance in predicting turbulent flow over a 13 percent-thick general-aviation airfoil (GA(W)-2). The isotropic eddy-viscosity $K-\varepsilon$ model of Speziale, Abid, and Anderson (SAA)[5] is one of the models; the other is the explicit algebraic stress model (EASM) presented in the last section. The incompressible ($M_\infty = 0.15$) experimental data of McGhee *et al.*[1] is used to assess

the models in predicting the aerodynamic characteristics of the airfoil over a range of chord Reynolds numbers.

In the three cases studied ($Re = 2.1 \times 10^6$, 4.3×10^6, and 6.3×10^6), the experimental transition point is fixed at 7.5 percent chord. In the computations, such a forced transition is difficult to implement in an unambiguous manner; however, in the computations, because transition occurred near the experimental transition point, no additional forcing was necessary.

Pressure variations over the airfoil at $Re = 4.3 \times 10^6$ at angles of attack of $0°$ and $18°$ are shown in Figure 1. At $\alpha = 0°$, both models predict essentially the same pressure distribution in the aft portion of the airfoil. Near the leading edge on the upper surface, the acceleration of the flow predicted by the $K - \varepsilon$ model is stronger than that predicted by the EASM; and on the lower surface a weaker acceleration is predicted by the $K - \varepsilon$ model. In both cases, the EASM is more accurate in predicting the experimental results. At the higher angle of attack, the predictions from both models are similar and replicate the experimental results well.

An important aspect of this study is to assess the ability of the models to correctly reproduce the lift and drag characteristics of the airfoils at different angles of attack and at different Reynolds numbers. Figure 2 shows the computed lift and drag coefficients for various angles of attack ($\alpha = 0°$, $8°$, $14°$, $16°$, and $18°$) at $Re = 2.1 \times 10^6$. At this chord Reynolds number, both models correctly predict the stall location; however, the EASM performs better than the $K - \varepsilon$ model in predicting the magnitude of C_l; the largest departure from the experimental values occurs at the higher angles of attack. This result is in contrast to the previous computational studies[2-4] on the ONERA-A airfoil at the same Reynolds number. In these earlier studies, the $K - \varepsilon$ model was unable to accurately predict the correct stall angle, and, in fact, did not predict stall at all over the range of angle of attack examined. This implies that the details of the airfoil shape are important factors in assessing whether a given turbulence model can predict a key aerodynamic characteristic of the airfoil.

The variation of C_d with C_l is shown in Figure 2(b). Note that the drag in the experiment was determined from a wake-rake (1.17 chords high) survey located 1 chord length downstream of the airfoil trailing edge. In the computation, the drag was deduced from the pressure and viscous force distribution along the airfoil. Nevertheless, at $\alpha = 0°$, and to a lesser extent $\alpha = 8°$, the computational results compare reasonably well with experimental results. However, at higher angles of attack, the computational results are quantitatively different than those of the experiment. It

is not possible to verify whether the wake-rake in the experiment was sufficiently far downstream to completely capture the entire wake region at the higher angles of attack. An analysis of the computed flow field at 1 chord downstream from the trailing edge indicated that the rake would not have been sufficient to span the entire wake region. This would have led to an underprediction of the drag. Because the experiment was performed in a wind tunnel which was approximately 3.75 chords high, while the computations were performed in a free-field with computational boundaries at 15 chords, the possibility arises that in the experiment the rake survey was adequate because the wall boundaries would require the flow to turn parallel to the walls and thus modify the wake. Unfortunately, it is not possible to conclusively isolate the cause of this drag prediction discrepancy at the higher angles of attack within the scope of the present study.

Figure 3 shows the predicted C_l and C_d for $Re = 4.3 \times 10^6$. At the lower angles of attack ($\alpha = 0°$ and $8°$), the EASM and to a slightly lesser extent the $K - \varepsilon$ model, does a good job in predicting C_l. At higher angles of attack ($\alpha = 16°$, $18°$, $20°$, and $22°$), both models do a poor job in predicting C_l. At $\alpha = 16°$ and $18°$, both models yield the same C_l, but at $\alpha = 20°$ and $22°$, the EASM prediction for C_l is less than that for the $K - \varepsilon$ model and is closer to the experimental results. Overall, neither model is capable of accurately predicting the C_l near stall.

As at the lower Reynolds number, C_d is predicted reasonably well at $\alpha = 0°$ and $8°$; however, at the higher angles of attack, the predictions differ significantly. The previous discussion on the C_d predictions at the lower Reynolds number is, of course, still applicable and would significantly contribute to any discrepancy.

At the highest Reynolds number studied ($Re = 6.3 \times 10^6$), the trends for both C_l and C_d are the same as for $Re = 4.3 \times 10^6$. Figure 4(a) shows that at $\alpha = 0°$ and $8°$, both models correctly predict the C_l; at the larger angles of attack ($\alpha = 15°$, $17°$, $19°$, and $21°$), neither model accurately predicts the C_l levels. The EASM yields results that are closer to the experimental levels than those of the $K-\varepsilon$ model; however, these predictions are still not acceptable. In addition, the stall angle predicted with the EASM is shifted slightly from both the $K-\varepsilon$ model predictions and the experimental value.

Consistent with results at the other two Reynolds numbers, the comparisons of the C_d predictions shown in Figure 4(b) are disappointing. At the higher angles of attack, neither model agrees with the experimental C_d results.

These results indicate that the turbulence models used in this study are incapable of predicting the correct airfoil aerodynamic characteristics at higher angles of attack

over the Reynolds-number range studied. A clearer picture of this Reynolds-number scaling effect is shown in Figure 5 in which the observed experimental behavior can be seen to be linear over the range of Reynolds-numbers studied. The $K-\varepsilon$ model displays neither the correct slope nor linear behavior in this region, which suggests that a key physical element is not being correctly incorporated into either the calculation or the turbulence model. The EASM also predicts the incorrect slope; however, the variation across the Reynolds-number range is much closer to linear than for the $K-\varepsilon$ model. Nevertheless, in both computations the qualitative features are predicted inaccurately.

An explanation for the $C_{l\max}$ predictions can be obtained from an analysis of the separation zone at the trailing edge of the airfoil. Unfortunately, the experimental study did not include any measurements or visualization of the flow-field near the airfoil trailing edge. Figure 6 shows the separation zone predicted by each model along the trailing edge of the upper surface near the stall angle of the EASM . At $Re = 2.1\times 10^6$, the isotropic model does not predict a separation zone along the surface which is consistent with the results of Lien and Leschziner[4]; however, the EASM is found to predict separation along the airfoil. When compared to Figure 2, it is seen that the EASM performs reasonably well in reproducing both the qualitative and quantitative features of the experiment up to the stall angle. As angle of attack increases, both models overpredict the C_l value; however, with the EASM predictions, are in better agreement with the experimental results. The lack of a predicted separation zone along the airfoil by the $K-\varepsilon$ model suggests that the earlier studies[2-4] at this Reynolds number may have completely missed the correct flow behavior along the upper surface.

Figure 6 shows separation zones predicted along the surface by both models at the intermediate Reynolds number $Re = 4.3\times 10^6$. Figure 3 shows in this case that the $K-\varepsilon$ model predicts the stall angle more accurately; the EASM overpredicts the separation zone at this Reynolds number (Fig. 6). This correlation of separation-zone size and lift coefficient suggests that at higher angles of attack both models grossly overpredict the size of the separation zone near the trailing edge. At this point in the analysis, the results are ambiguous. At $Re = 2.1\times 10^6$, the $K-\varepsilon$ model does not predict separation along the airfoil and, therefore, poorly predicts the C_l distribution near stall. However, at $Re = 4.3\times 10^6$ the EASM overpredicts the separation-zone size and, therefore, underpredicts the C_l distribution near stall.

The results for $Re = 6.3\times 10^6$ are also shown in Figure 6. In this case, the EASM more closely approximates the experimental C_l distribution near stall (Fig.

4), although the stall angle is underpredicted by both models. Thus, the size of the separation zone is underpredicted by the $K-\varepsilon$ model (Fig. 6). Because both models overpredict the C_l distribution at angles of attack greater than the stall angle, it can be assumed that at these higher angles of attack the separation-zone size would be underpredicted by both models. The reduction in separation-zone size near the trailing edge, between the $Re = 4.3 \times 10^6$ and 6.3×10^6 cases, correlates with the decrease in $C_{l\max}$ shown in Figure 5.

The results presented in this study have shown that neither the isotropic eddy-viscosity $K-\varepsilon$ model nor the EASM accurately predict the lift and drag coefficients over a range of Reynolds numbers and angles of attack. However, areas in which the models do perform well relative to one another and in comparison with experiment have been identified. Of course, other two-equation $K-\varepsilon$ models and other ASM's are available for testing; however, while the quantitative results may change slightly, the overall qualitative performance characteristics are not expected to change significantly. The question then remains to identify which aspect of flow-field physics is not being properly modeled. Unfortunately, with the limited amount of mean field experimental data available this becomes problematic.

Although the turbulence models themselves may be inadequate, other dynamic features of the flow also may not have been properly accounted for and may need to be investigated. One such feature of the experimental flow field, which was not incorporated into the present study, is the unsteady shedding from the trailing edge that occurred at and above the intermediate chord Reynolds number (R. J. McGhee, private communication). The present numerical procedure does not solve the governing equations in a time-accurate manner and as such cannot give a true representation of the time-dependent behavior near the airfoil trailing edge. This unsteadiness may affect the separation-zone size, which would result in a different average picture of the airfoil characteristics. Some evidence that an important dynamic feature of the flow field has been omitted from the calculations can be seen in Figure 5. The linear behavior of C_{lmax} versus Re displayed between $Re = 2.1 \times 10^6$ and 4.3×10^6 (and throughout the Reynolds-number range for the experimental data) is lost at the higher Reynolds number, which suggests that some aspect of the physics may have been omitted.

IV CONCLUDING REMARKS

This purpose of this study was to begin a systematic evaluation of the predictive capabilities of two distinct types of turbulence closure models in predicting the aero-

dynamic characteristics of airfoils at different Reynolds numbers. One of the models was an isotropic eddy-viscosity $K-\varepsilon$ model; the other was an explicit algebraic stress model (EASM). These two models were computationally equivalent in both time and memory requirements but were based on significantly different physics. As such, the study was not intended to focus on a particular turbulence model within each type but on the predictive capabilities of a particular type of model. The selection of a different model within each type may have yielded slightly different quantitative results, but the overall conclusions would not have differed significantly.

Neither type of model accurately computed the lift and drag characteristics over the Reynolds-number range studied. The EASM more closely predicted the C_l distributions over a wider range of angle of attack for a particular Reynolds number but was unable to accurately predict the distributions near stall. A similar conclusion was reached for prediction of the drag coefficient over the Reynolds-number range studied, although other factors related to the differences between the computational and experimental problems may explain some of these.

The separation zone at the airfoil trailing edge near stall was also examined at the three Reynolds numbers. The predicted separation-zone sizes varied significantly among the models; these results were correlated with the lift distributions at the three Reynolds numbers. Unfortunately, no unique feature could be identified that would indicate the reason for the poor predictive performance of the models at higher angles of attack. However, one possible key feature of the experimental study, that has not been accurately represented in this study is the unsteady shedding from the airfoil trailing edge. Shedding would affect the separation-zone size predicted by the different models and could lead to different average values for C_l and C_d. The next phase of this study will address this issue by performing these same calculations with a time-accurate numerical solver.

REFERENCES

[1]McGhee, R. J.; Beasley, W. D.; and Somers, D. M.: *Low-Speed Aerodynamic Characteristics of 13-Percent-Thick Airfoil Section Designed for General Aviation Aviation Applications.* NASA TM X-72697, 1977.

[2]Davidson, L.; and Rizzi, A.: *Navier-Stokes Computation of Airfoil in Stall Using Algebraic Reynolds-Stress Model.* AIAA Paper No. 92-0195, 1992.

[3]Davidson, L.: Prediction of the Flow Around an Airfoil Using a Reynolds Stress Transport Model. *Transactions of the ASME Journal of Fluids Engineering,* vol. 117, 1995, pp. 50–57.

[4]Lien, F. S.; and Leschziner, M. A.: Modelling 2D Separation from a High Lift Aerofoil with a Non-Linear Eddy-Viscosity Model and Second-Moment Closure. *Aeronautical Journal*, vol. 99 no. 984, 1995, pp. 125–144.

[5]Speziale, C. G.; Abid, R.; and Anderson, E. C.: Critical Evaluation of Two-Equation Models for Near-Wall Turbulence. *AIAA J.*, vol. 23 no. 9, 1992, pp. 1308–1319.

[6]Gatski, T. B.; and Speziale, C. G.: On Explicit Algebraic Stress Models for Complex Turbulent Flows. *J. Fluid Mech.*, vol. 254, 1993, pp. 59–78.

[7]Speziale, C. G.; and Gatski, T. B.: *Analysis and Modeling of Anisotropies in the Dissipation Rate of Turbulence.* Submitted for Publication, 1996.

[8]Xu, X. H.; and Speziale, C. G.: *An Explicit Algebraic Stress Model of Turbulence with Anisotropic Dissipation.* Technical Report No. AM-96-003, Boston University, Boston, MA, 1996.

[9]Speziale, C. G. Analytical Methods for the Development of Reynolds-Stress Closures in Turbulence. *Annu. Rev. Fluid Mech.*, vol. 23, 1991, pp. 107–157.

[10]Hanjalić, K.: Advanced Turbulence Closure Models: A View of Current Status and Future Prospects. *Int. J. Heat Fluid Flow*, vol. 15 no. 3, 1994, pp. 178–203.

[11]Gatski, T. B.: Turbulent Flows: Model Equations and Solution Methodology, *Handbook of Computational Fluid Mechanics,* (R. Peyret, ed.), Academic Press, Inc., London, 1996.

[12]Gatski, T. B.; Hussaini, M. Y.; and Lumley, J. L. (eds.): *Simulation and Modeling of Turbulent Flows*, Oxford University Press, New York, 1996.

[13]Speziale, C. G.; Sarkar, S.; Gatski, T. B.: Modeling the Pressure-Strain Correlation of Turbulence: An Invariant Dynamical Systems Approach. *J. Fluid Mech.*, vol. 227, 1991, pp. 245–272.

[14]Abid, R.; Rumsey, C.; and Gatski, T. B.: Prediction of Nonequilibrium Turbulent Flows with Explicit Algebraic Stress Models. *AIAA J.* vol. 33 no. 11,1995, pp. 2026–2031.

[15] Abid, R.; Morrison, J. H.; Gatski, T. B.; and Speziale, C. G.: Prediction of Complex Aerodynamic Flows with Explicit Algebraic Stress Models. AIAA Paper No. 96-0565, 1996.

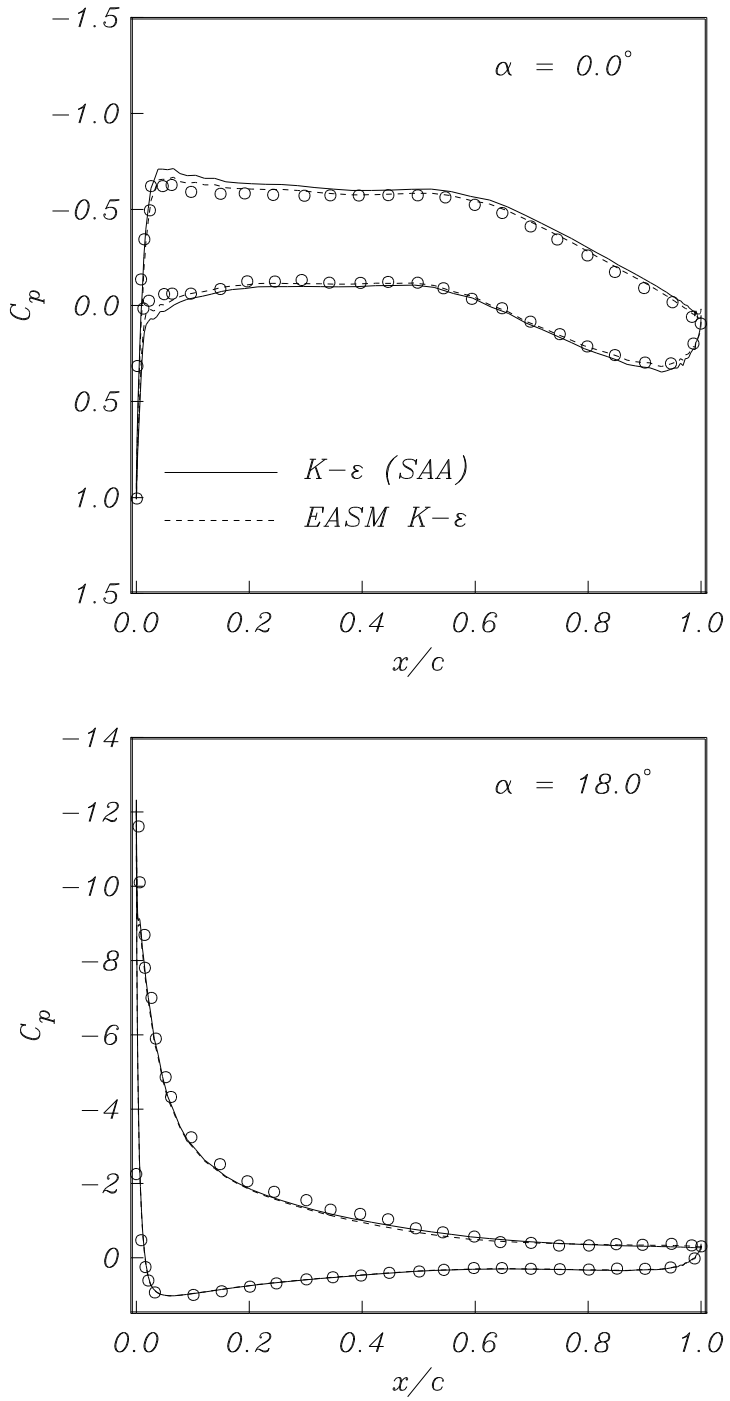

Figure 1. Pressure variation around airfoil at $\alpha = 0°$ and $18°$ with $Re = 4.3 \times 10^6$.

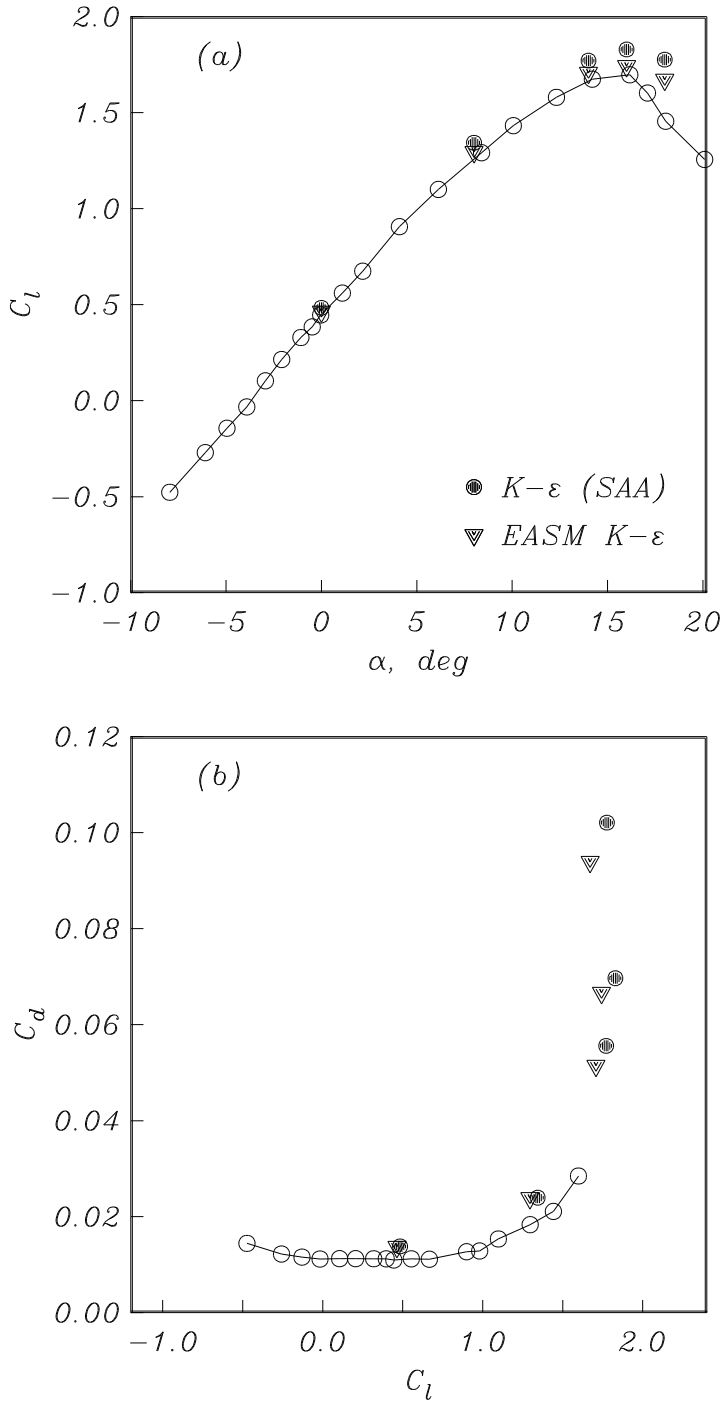

Figure 2. Lift and drag airfoil characteristics at $Re = 2.1 \times 10^6$. (a) Variation of lift coefficient with angle of attack, (b) Variation of drag and lift coefficients.

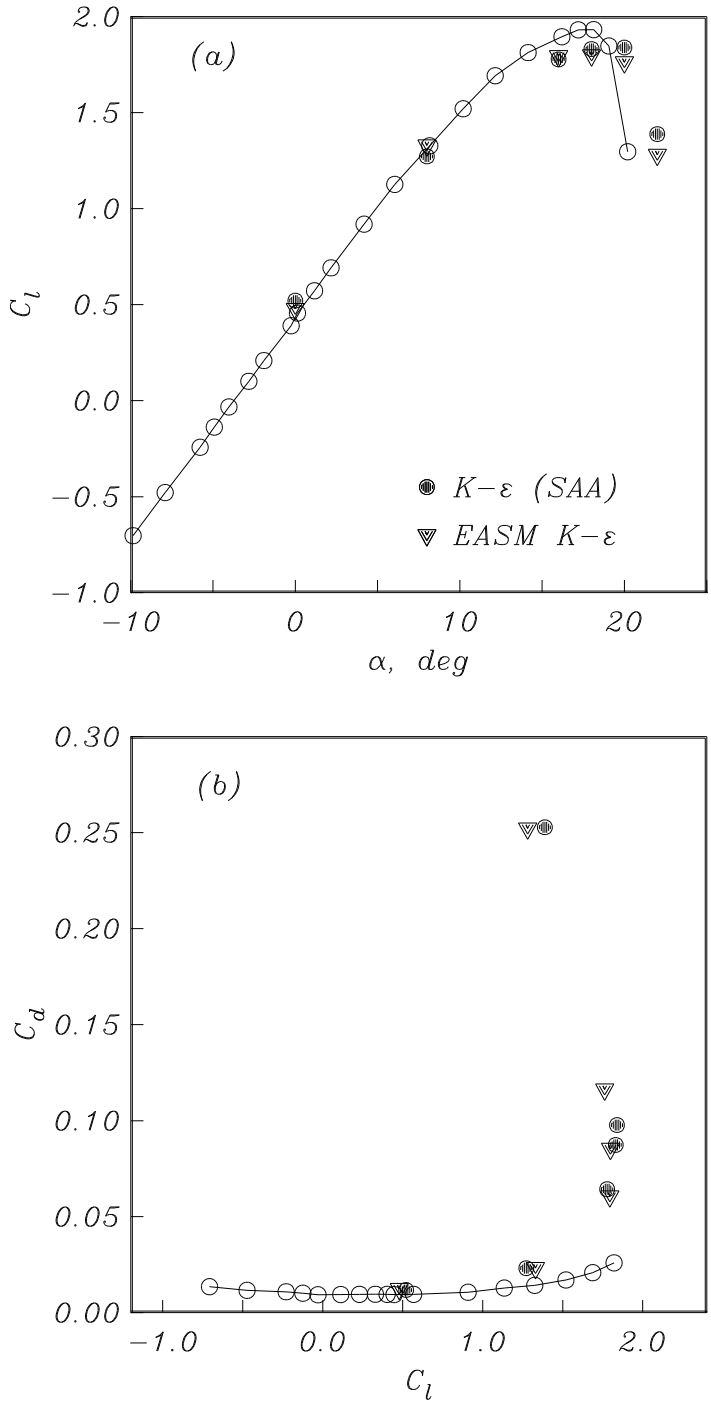

Figure 3. Lift and drag airfoil characteristics at $Re = 4.3 \times 10^6$. (a) Variation of lift coefficient with angle of attack, (b) Variation of drag and lift coefficients.

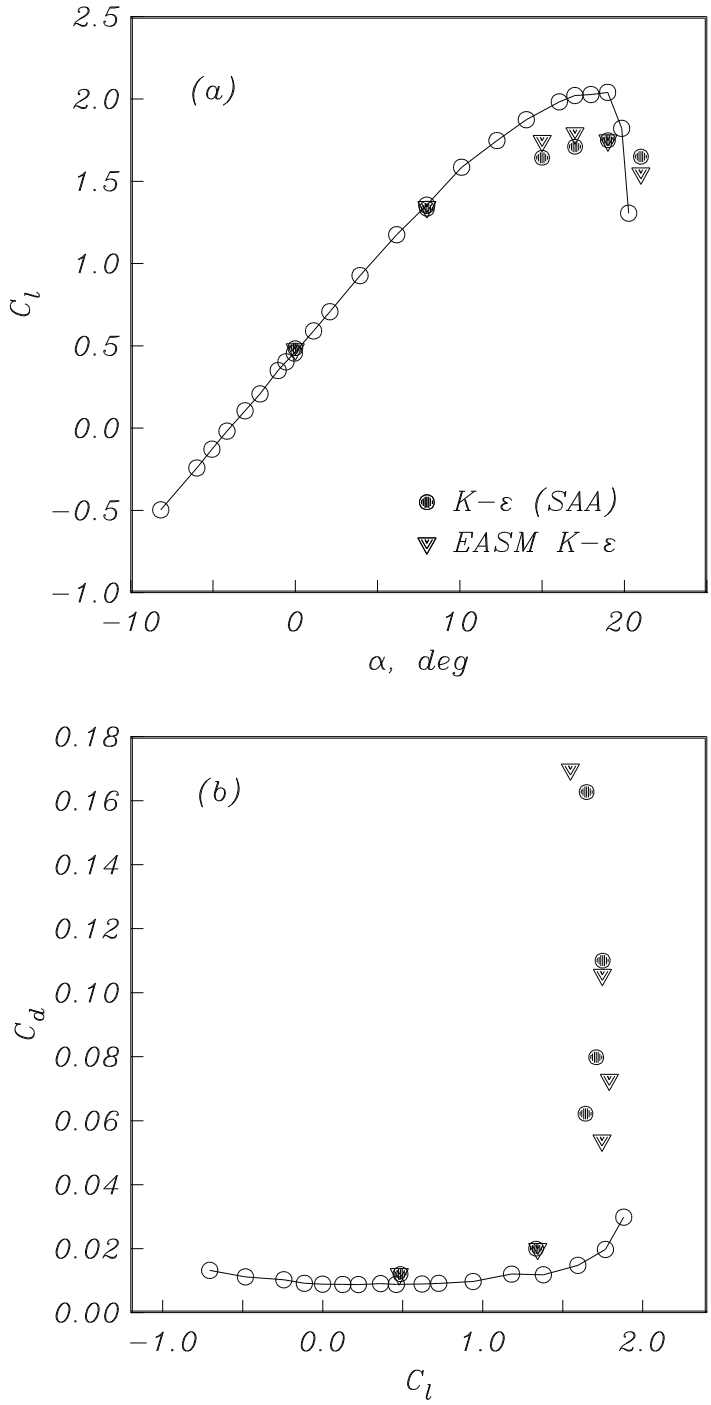

Figure 4. Lift and drag airfoil characteristics at $Re = 6.3 \times 10^6$. (a) Variation of lift coefficient with angle of attack, (b) Variation of drag and lift coefficients.

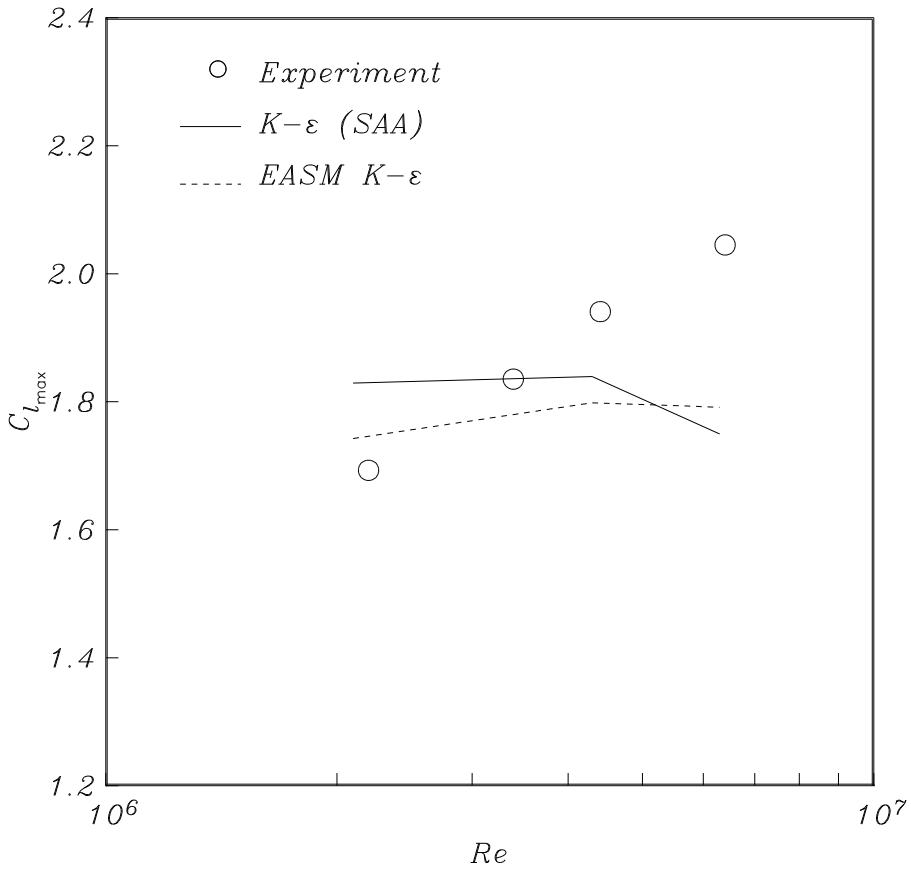

Figure 5. Variation of maximum lift coefficient with Reynolds number.

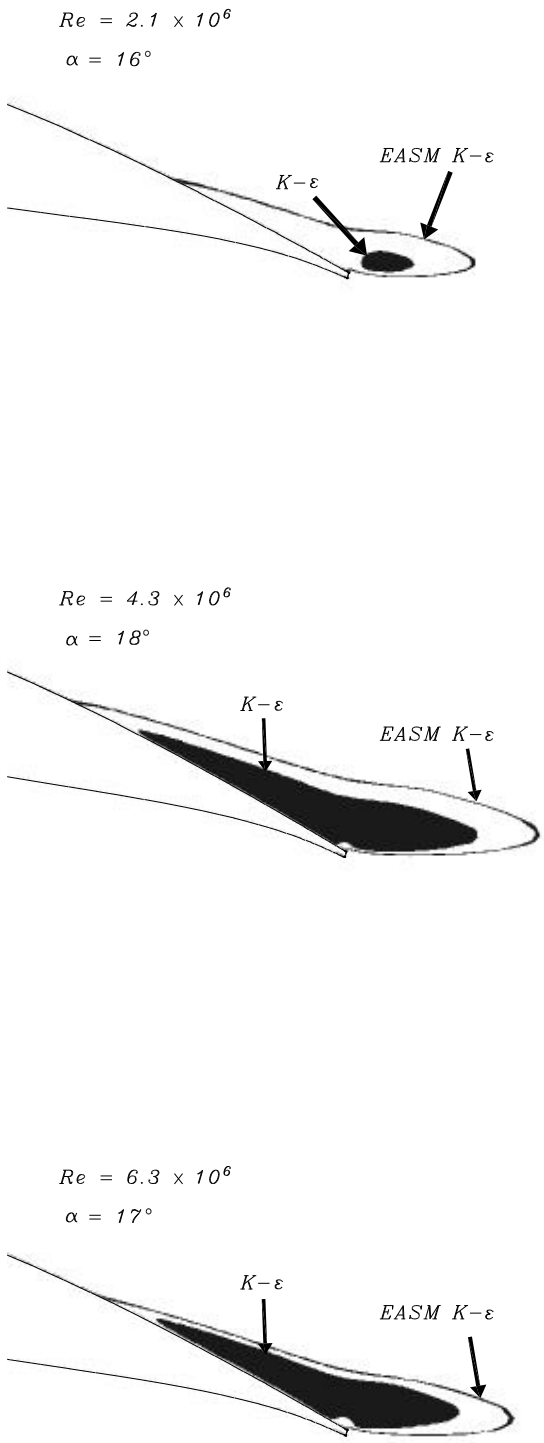

Figure 6. Comparison of stall separation-zone size at airfoil trailing edge.